Nonlinear Arrhenius behavior of self-diffusion in β-Ti and Mo

Yaxian Wang,[1,2,*] Zhangqi Chen,[1,*] Wolfgang Windl,[1,†] and Ji-Cheng Zhao[3,‡]

[1]*Department of Materials Science and Engineering, The Ohio State University, 2041 College Road, Columbus, Ohio 43210, USA*
[2]*Beijing National Laboratory for Condensed Matter Physics and Institute of Physics, Chinese Academy of Sciences, Beijing 100190, China*
[3]*Department of Materials Science and Engineering, University of Maryland, 4418 Stadium Drive, College Park, Maryland 20742, USA*

(Received 27 October 2021; accepted 23 May 2022; published 7 June 2022)

While anomalous diffusion coefficients with non-Arrhenius-like temperature dependence are observed in a number of metals, a conclusive comprehensive framework of explanation has not been brought forward to date. Here, we use first-principles calculations based on density functional theory to calculate self-diffusion coefficients in the bcc metals Mo and β-Ti by coupling quasiharmonic transition state theory and large-displacement phonon calculations and show that anharmonicity from thermal expansion is the major reason for the anomalous temperature dependence. We use a modified Debye approach to quantify the thermal expansion over the entire temperature range and introduce a method to relax the vacancy structure in a mechanically unstable crystal such as β-Ti. The effect of thermal expansion is found to be crucial for the nonlinear, non-Arrhenius "anomalous" self-diffusion in both bcc systems, with β-Ti showing a 60% larger relative nonlinearity parameter than Mo. Our results point to temperature dependence in the diffusion prefactor from thermal expansion as the major origin of anomalous self-diffusion. The methodology proposed for β-Ti is general and simple enough to be applicable to other mechanically unstable crystals.

DOI: 10.1103/PhysRevMaterials.6.063402

I. INTRODUCTION

Self-diffusion in metals is believed to be understood rather well and their coefficients (D) obey a linear temperature (T) dependency on an Arrhenius plot ($\ln D$ vs $1/T$). However, a number of elements show a remarkable "curvature" and thus deviation from linearity. Although such an anomaly is rare for non-bcc metals, it has been found to be especially strong in the group IVB metals Ti, Zr, and Hf, whose bcc phases are mechanically unstable at lower temperatures, while it is much weaker in other bcc metals like Mo and Nb that are mechanically stable for all temperatures [1].

Focusing on bcc Mo (in the following "Mo") and bcc Ti (in the following "β-Ti") as prototypes for mechanically stable and unstable bcc metals, the underlying mechanism(s) for such a non-Arrhenius behavior has been under debate for many decades and remains unsettled. Given that self-diffusion in elementary metals is governed by vacancy jumps, initial explanations were mostly based on the contribution of "secondary" diffusion mechanisms and include diffusion via divacancies [2], next-nearest-neighbor (NNN) jumps [3,4], diffusion via interstitials [5], or diffusion enhancement by phase transformations [6,7]. While none of these mechanisms could be conclusively confirmed for either Mo or β-Ti, it has been argued in the late 1980s that secondary mechanisms would not be consistent with experiments [8,9], and it was suggested that self-diffusion should be dominated by the traditional monovacancy jumps through nearest-neighbor (NN) sites in both Mo and β-Ti [9–11]. This would leave some form of anharmonicity as the explanation for the diffusion anomaly, since within harmonic transition state theory [12,13], the temperature dependence of the diffusion coefficient should exactly follow the Arrhenius equation $D(T) = D_0 \exp(-E_0/k_B T)$ with temperature-independent prefactor D_0 and activation energy E_0, which for monovacancy diffusion is the sum of vacancy formation enthalpy E_f and migration enthalpy E_m. The anharmonicity was initially suggested to manifest itself in the form of soft phonons due to the specific distribution of the d electrons [14,15].

By now, the continuous advances in atomistic simulation methods and computational capabilities have provided new opportunities to gain insight into the microscopic origin of anomalous diffusion, and lead to a variety of explanations for non-Arrhenius diffusion. Proposed mechanisms include a vacancy-interstitial model in β-Ti [16], anharmonic effects in both β-Ti [17] and in Mo [18], and concerted atomic motion [19,20].

The previous work has been performed either with classical molecular dynamics (MD) based on empirical potentials or with density functional theory (DFT). On the classical MD side, in Ref. [16] diffusion coefficients in β-Ti were determined from the mean-square displacement of the atoms. The results suggested that interstitials would play a non-negligible role at self-diffusion near melting temperature and the sum of Arrhenius-like vacancy and interstitial diffusions with different slopes would result in the observed anomalous diffusion. The spontaneous formation of Frenkel pairs was also found in Ref. [20], leading to temperature-dependent formation energies. While no diffusion coefficients were calculated in Ref. [20], it was argued that the temperature-dependent formation energy would give rise to anomalous diffusion. The

*These authors contributed equally to this work.
†windl.1@osu
‡jczhao@umd.edu

fact that the high-temperature defect concentrations varied by several orders of magnitude between Refs. [16] and [20] as well as the fact that interstitial concentrations have been found exceedingly small in Mo even at its melting temperature casts doubt on this explanation. In another MD study [19], it was proposed that concerted motion of atoms significantly contributed to diffusion at temperatures >83% of the melting temperature, in addition to the otherwise dominant vacancy diffusion which followed a straight Arrhenius behavior over the entire examined temperature range from 73% to 97% of the melting temperature. While the considerable variation in results of these studies may at least partially originate from the different interatomic potentials used [21–23], the fact that experiments show pronounced nonlinearity already in the sub-1600 K range where all MD studies find Arrhenius-like behavior makes further studies desirable.

Other than classical MD, DFT-based methods do not rely on empirical interatomic potentials. Performing harmonic transition state theory based DFT calculations of diffusion coefficients started to become standard in the late 1990s for semiconductors [24] and were adopted into the metallic systems a decade later [25–28]. Mattson *et al.* [18] proposed a large quadratic temperature dependence of the vacancy formation energy in bcc Mo based on *ab intio* molecular dynamics (AIMD) simulations, but did not study the temperature dependence of the formation entropy. Their results consist only of two data points obtained at >2400 K and the zero-temperature value, thus are insufficient to quantify the nonlinearity over a wide temperature range. Non-MD-based first-principles calculations on the high-temperature bcc phases of group IVB metals like titanium, zirconium, and hafnium have remained quite challenging due to their mechanical instability at zero temperature [29,30], with a manifestation of decreasing energies and negative curvatures as a function of atomic displacement [30] or strain [29] in certain directions at 0 K. Since phonon frequencies are determined by square roots of energy versus displacement curvatures, this corresponds to vibrational modes with imaginary frequencies. Since within the common harmonic or quasiharmonic approximations, vibrational free energies in solids are calculated from phonon frequencies, the appearance of imaginary frequencies impedes free-energy calculations at finite temperatures for mechanically unstable crystals.

A number of approaches have been suggested to overcome the limitations from mechanical instabilities through molecular dynamics [31] or phonon calculations on cells with self-consistently displaced atoms [32] to capture the temperature-induced anharmonicity, but most of them are computationally too expensive to perform calculations on supercells with point defects. Kadkhodaei *et al.* employed a combination of self-consistent *ab initio* lattice dynamics (SCAILD) and the temperature-dependent effective potential (TDEP) method and examined in a thorough study the influence of phonon anharmonicity on the diffusion coefficient [17] in β-Ti. They obtained much improved self-diffusion coefficients of β-Ti in comparison to the harmonic approach. However, their work did not include thermal expansion, which we will show in this work to be the prime suspect to cause anomalous diffusion, and left the lattice parameters fixed, resulting in an almost linear relation between $\ln D$ and $1/T$.

Herein, we perform a comprehensive study of the thermal expansion and self-diffusion anomaly in the mechanically stable Mo and the unstable β-Ti with an accurate and efficient *ab initio* approach. Our work utilizes the large-displacement method (LDM), first proposed by Antolin *et al.* [30], from which we demonstrate that the thermal expansion coefficients are well captured in the temperature range where the quasiharmonic approximation (QHA) applies. For the minimum-volume at each temperature, we then calculate the free energy of vacancy formation and diffusion coefficients within LDM-based harmonic transition state theory, effectively forming a quasiharmonic version of it. Our predicted self-diffusion coefficients are within the range of previous measurements, and their anomalous temperature dependence in both Mo and β-Ti strongly indicates that going beyond harmonic to quasiharmonic transition state theory can explain anomalous temperature dependence of self-diffusion in a natural way that eliminates the need to invoke *ad hoc* nontraditional assumptions about the diffusion mechanism. Finally, we quantify the deviation from the Arrhenius dependence using a previously proposed *nonlinearity* parameter [33] and discuss our findings in light of both previous experimental data and computational work. Our results show strong evidence that nonlinear Arrhenius self-diffusion arises mostly from thermal expansion, and further pinpoint that it is not the migration enthalpy, but the formation entropy and, in the case of β-Ti, attempt frequency that carries the majority of the temperature dependence. This work sheds new light on the nature of anomalous self-diffusion in Mo and β-Ti, and validates that LDM is an effective way to perform such calculations in mechanically unstable metals.

II. METHODOLOGY

A. Self-diffusion theory for the bcc lattice

In the monovacancy mechanism of self-diffusion in the bcc lattice, the atom-vacancy exchange jump happens between two nearest-neighbor positions along $\frac{1}{2}[111]$. The bcc self-diffusion coefficient can be written as

$$D = gfa^2 C_v \Gamma, \tag{1}$$

where g is the geometrical factor (1 for cubic lattices), f the correlation factor (0.7272 for bcc [34,35]), a the lattice constant, C_v the vacancy concentration, and Γ the atom-vacancy exchange jump frequency along $\frac{1}{2}[111]$.

The atomic fraction of vacancy lattice sites C_v is given by

$$C_v = \exp\left(-\frac{\Delta G_f}{k_B T}\right) = \exp\left(\frac{\Delta S}{k_B}\right)\exp\left(-\frac{\Delta H_f}{k_B T}\right), \tag{2}$$

where ΔG_f is the free energy of vacancy formation within the bcc lattice. ΔS_f and ΔH_f are the vacancy formation entropy and enthalpy, respectively. The atom-vacancy exchange jump frequency Γ can be calculated within transition state theory as [36]

$$\Gamma = \nu^* \exp\left(-\frac{\Delta H_m}{k_B T}\right), \tag{3}$$

where ΔH_m denotes the migration enthalpy and ν^* the attempt frequency. Substituting Eqs. (2) and (3) into Eq. (1), the

self-diffusion coefficients in bcc metals can be calculated by

$$D(T) = \overbrace{0.7272a^2\nu^* \exp\left(\frac{\Delta S_f}{k_B}\right)}^{D_0} \exp\left(-\frac{\overbrace{\Delta H_f + \Delta H_m}^{E_0}}{k_B T}\right). \tag{4}$$

Therefore, four parameters will be calculated to obtain self-diffusion coefficients through DFT calculations: ΔH_f, ΔS_f, ΔH_m, and ν^*. Of those, ΔH_f and ΔH_m contribute to the thermal activation energy E_0, while ΔS_f and ν^* contribute to the prefactor D_0.

We will describe the methodology to compute these parameters from *ab initio* in Sec. II B. Before that, in practice the vacancy structures of Mo and β-Ti need to be relaxed, which is a straightforward task for Mo, but requires some extra attention for Ti and techniques such as the large-displacement method (Sec. II C), which we will discuss in Sec. II D. Section II E summarizes the calculation of thermal expansion within QHA, followed by descriptions of the nonlinearity parameter (Sec. II F), overall procedure (Sec. II G), and computational details of DFT calculations (Sec. II H).

B. Calculation of the diffusion coefficient

Formation quantities such as ΔG_f, ΔS_f, or ΔH_f can be calculated by the respective difference between the perfect supercell and the relaxed cell with one vacancy. As an example,

$$\Delta G_f = G(X_{N-1}V_1) - \frac{N-1}{N} G(X_N), \tag{5}$$

where X is the lattice atom, V indicates a vacancy, and N indicates the number of lattice sites in the supercell.

In order to calculate the vibrational contribution to the free energies of formation at finite temperatures, $F_f(T)$, and the entropy of formation, $S_f(T)$, we use the quasiharmonic approximation (QHA) [37] based on supercell Γ-point calculations as described in previous work [38]. There, the entropy is approximated by

$$S(V,K) = k\left\{ \int \frac{\frac{h\nu}{k_B T}}{\exp(\frac{h\nu}{k_B T}) - 1} g[\nu(V)] d\nu - \int g[\nu(V)] \ln\left[1 - \exp\left(-\frac{h\nu}{k_B T}\right)\right] d\nu \right\}, \tag{6}$$

where $g[\nu(V)]$ is the phonon density of states [38] and the Γ-point phonon frequencies $\nu(V)$ are calculated for a supercell with volume V.

The attempt frequency ν^* can be calculated as

$$\nu^* = \prod_{i=1}^{3N-3} \nu_i \Big/ \prod_{j=1}^{3N-4} \nu_j, \tag{7}$$

where ν_i and ν_j are the normal-mode (Γ-point phonon) frequencies of the stable and saddle point configurations, respectively, for a system of N atoms and one vacancy. The product in the denominator specifically excludes the (imaginary) frequency corresponding to the unstable mode at the transition state.

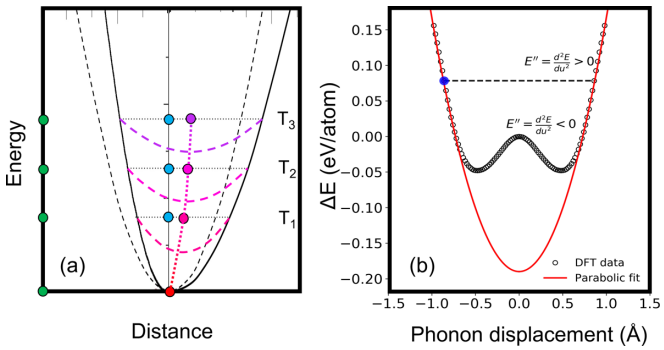

FIG. 1. (a) Schematic representation of the effect of thermal expansion on vibrational properties for atoms in a harmonic (dashed black line) vs an anharmonic (solid black line) potential. As the temperature increases, the system gains kinetic energy, and states with higher energy on the energy landscape are sampled. The equilibrium position of atoms is the "midpoint" of the potential wall. The harmonic potential is symmetric, and the equilibrium bond length of the atom (distance between green and blue circles) does not change with temperature, whereas the bond length in the anharmonic potential increases (distance between green and red/purple circles). At the same time, the curvature of the quasiharmonic potentials (red/purple dashed lines) decreases with increasing temperature. (b) Energy difference with respect to the perfect cell in a frozen-phonon cell for the unstable N-point displacement pattern as a function of displacement (black circles) in β-Ti. The energy "hump" at zero displacement corresponds to the mechanical instability, i.e., a negative curvature $E'' < 0$, at zero temperature. A harmonic potential well (red curve) is obtained by matching energy and curvature of the energy data at the large-displacement value of 0.88 Å proposed in Ref. [30]. This represents the high-temperature regime (black dashed line), where the atomic vibration exhibits large amplitude (blue marker) with high thermal energy, resulting in real phonon frequencies ($E'' > 0$) governed by the envelope harmonic potential.

According to Eq. (4), the dependence of $\ln D$ vs $1/T$ will be perfectly Arrhenius based on harmonic transition state theory, where the atoms oscillate in perfect harmonic (parabolic) energy wells, and the energy landscape around the transition state is also perfectly parabolic. Within these assumptions, thermal expansion is zero and the Arrhenius plot is perfectly linear. Anharmonicities, which are deviations of any kind from parabolicity, are the most likely, if not the only, possible explanation for nonlinear Arrhenius behavior in this situation. The thorough work by Kadkhodaei *et al.* [17] includes the phonon-anharmonicities in a very complete way. However, thermal expansion was not included in that work. Since thermal expansion is directly proportional to the Grüneisen parameter, which is the most widely used quantitative measure of anharmonicity [39], thermal expansion thus becomes the most likely candidate to cause anomalous diffusion. In order to include thermal expansion into our calculations, all four parameters in Eq. (4) that determine the diffusivity need to be calculated for simulation cells whose volume increases with temperature, which methodically corresponds to the QHA. For example, when a single atom vibrates in an anharmonic energy potential [Fig. 1(a), solid curve], the equilibrium atomic position, here represented by the bond length, increases with temperature in comparison to the harmonic case

[Fig. 1(a), dashed parabola], resulting in enthalpy gain due to the elastic energy. Meanwhile, the effective curvature [$E'' =$ average(E''_{left}, E''_{right}) in the schematic of Fig. 1(a)] of the anharmonic potential that determines the vibrational frequencies also changes with temperature as higher potential energies are sampled due to the increased kinetic energy, affecting both hopping frequency [Eq. (7)] and entropy [Eq. (6)]. In most cases the relative change of phonon frequencies of the initial vs saddle point configuration (attempt frequency) and vacancy vs perfect configuration (formation entropy) cancels out so that QHA does not lead to a significant nonlinearity in the ln D vs $1/T$ relation. However, we show here that consideration of the previously neglected effect of thermal expansion is crucial to capture the anomalous diffusion in bcc metals, and for β-Ti more so than for Mo.

The climbing image nudged elastic band method (CI-NEB) [40] with 3 images was employed to determine the transition state (saddle point) structures for Mo and Ta (see Sec. II D why Ta), with the saddle point configuration of Ti determined from those as described in the following section due to the relaxation problems in mechanically unstable high-temperature structures. The initial and final structures, i.e., stable states, were fully relaxed first. Then during the CI-NEB calculations, all supercell volumes were fixed.

C. Large-displacement quasiharmonic transition state theory

The large-displacement method (LDM) treats the anharmonicity through large atomic displacements into the high-temperature anharmonic range of the atoms' energy wells. Within LDM, phonons are calculated from the curvature of the harmonic envelope [red curve in Fig. 1(b)] of the quartic energy-vs-displacement curve (circles). At high temperatures, or above the transition temperature, the atoms actually sample at large vibrational amplitudes, which makes them carry across the "hump" at zero displacement [black circles in Fig. 1(b)], i.e., the local energetic barrier, and thus overcomes the mechanical instability of the bcc phase, therefore eliminating all imaginary frequencies from the phonon dispersions. Technically, this approach thus works like any standard finite-difference phonon calculation with the exception that the displacements are one or two orders of magnitude larger. The only question there is how large the displacement should be. In Ref. [30], a large-displacement value of 0.88 Å was proposed for β-Ti, resulting in good agreement of theoretical and experimental phonon dispersion. The sensibility of this large-displacement value for β-Ti proposed is further confirmed by the comparison of the theoretical thermal expansion coefficients with the experimental values (Sec. III A). For Mo which is mechanically stable at zero temperature, regular moderately small displacements (we use 0.05 Å) are the most sensible choice as was also shown in Ref. [30].

D. Relaxation of vacancy structure for Ti

Due to β-Ti's mechanical instability, one cannot simply relax its supercell with one vacancy at zero temperature like is commonly done for other crystals to determine the ground state structure. If one tried, one would end up with unphysically large atomic displacements and a negative formation energy as shown in Sec. III B. Because of the same reason, the CI-NEB method also cannot be used to find the saddle point structure. To circumvent this problem, we first perform an approximate, nearest-neighbor (NN) only, relaxation based on free energies for Ti, where free-energy calculations based on the LDM (Sec. II C) at three different temperatures between phase transformation temperature (1150 K) and melting temperature (1940 K) were performed for differently displaced NN shells in an otherwise unrelaxed vacancy cell. The minimum-energy displacement was then linearly extrapolated to zero temperature, $d_{\text{Ti}}(T) = d^0_{\text{Ti}} + \vartheta T$. Since in the final calculations, we want to use full instead of NN-only relaxation, we now use the zero-temperature extrapolated value to identify an appropriate surrogate structure for Ti from other mechanically stable bcc materials, scaled to the correct lattice constant. For NN-only relaxation, Mo is found to have one of the smallest and Ta one of the largest relative NN relaxations. Thus, the positions of the atoms in the interpolated surrogate Ti cell can be calculated from

$$x_{\text{Ti}} = \frac{d^0_{\text{Ta}} - d^0_{\text{Ti}}}{d^0_{\text{Ta}} - d^0_{\text{Mo}}} x_{\text{Mo}} + \frac{d^0_{\text{Ti}} - d^0_{\text{Mo}}}{d^0_{\text{Ta}} - d^0_{\text{Mo}}} x_{\text{Ta}}, \tag{8}$$

a procedure that is easily transferable to other mechanically unstable bcc crystals. The saddle point structure of β-Ti is calculated in the same way from CI-NEB results for Mo and Ta. Results for these relaxation calculations are discussed in detail in Sec. III B.

E. Thermal expansion

In the quasiharmonic version of transition state theory we employ in this paper, the four variables that determine the self-diffusion coefficients according to Eq. (4) are ΔH_f, ΔS_f, ΔH_m, and ν^*. They are evaluated at the minimum-lattice constant in the Helmholtz free energy for each temperature, determined in turn from the traditional quasiharmonic approximation to vibrational entropy. The Helmholtz free energy of a system as a function of volume (V) and temperature (T) is expressed as

$$F(V,K) = E_{\text{tot}}(V) + k_B T \left\{ g[\nu(V)] h\nu d\nu + \int g[\nu(V)] \ln\left[1 - \exp\left(-\frac{h\nu}{k_B T}\right)\right] d\nu \right\}, \tag{9}$$

where E_{tot} is the total (internal) energy at 0 K, in addition to the quantities defined for Eq. (6). As described in Sec. II C, we used the LDM for the Ti phonon calculations and traditional displacements for Mo.

In order to determine the thermal expansion coefficient, we fit the lattice constant data vs temperature with a modified expression derived from the Debye model [41],

$$a(T) = a_0[1 + I_a(T) T \varphi(\theta_D/T)], \tag{10}$$

where a_0 is the lattice parameter at 0 K, θ_D is the Debye temperature, and φ is the Thacher function to approximate the Bose-Einstein weighted integral from the Debye specific heat, Eq. (6) from Ref. [42]. Other than in the original model, we give I_a a linear temperature dependence,

$I_a(T) = I_0(1 + \chi T)$ with I_0 and χ as fitting parameters in addition to θ_D, since I_a, originally given by $I_a = K\gamma k_B/V_0$ (K is the compressibility, γ the Grüneisen constant, and V_0 the minimum volume of the cell), should be temperature dependent because both Grüneisen parameter and elastic constants [43] are temperature dependent. Without this, the typically observed increase in thermal expansion with temperature in the high-temperature limit is not described well enough. The linear thermal expansion coefficient (α) is finally calculated by $\alpha = \frac{1}{a_0}\frac{\partial a}{\partial T}$ from the temperature derivative of Eq. (10).

F. Quantification of nonlinearity

In order to quantify the nonlinearity in our calculated and previous (experimental) data, we fit the logarithm of the diffusion coefficient in an Arrhenius plot with an equation analogous to bowing-parameter-dependent quadratic equations used for lattice parameters or elastic constants [44],

$$\ln D(\beta) = \frac{\beta - \beta_l}{\beta_h - \beta_l}\ln D_h + \frac{\beta_h - \beta}{\beta_h - \beta_l}\ln D_l + \eta\frac{(\beta - \beta_l)(\beta_h - \beta)}{(\beta_h - \beta_l)^2}. \quad (11)$$

There, the first two terms are the linear interpolation between the logarithms of highest (l) and lowest (l) diffusion coefficients (respectively, D_h and D_l can be fitting coefficients), $\beta = 1/k_BT$, and η is the "bowing parameter," i.e., the measure of the quadratic term, whose form is chosen to be zero at the extremal temperatures. An absolute nonlinearity parameter λ can then be used to compare the degree of nonlinearity between the different elements independently of whether the temperature ranges exactly overlap or not. Following Eqs. (3) and (9) in Ref. [33], we calculate λ by

$$\lambda = \frac{\eta}{\sqrt{30}|\ln D_h - \ln D_l|}. \quad (12)$$

G. Overall procedure

In order to determine the diffusion coefficients for Ti and Mo within the quasiharmonic transition state theory employed in this paper, we performed the following steps:

(1) The thermal expansion, i.e., the temperature dependence of the lattice constants, was calculated within the quasiharmonic approximation as described in Sec. II E based on perfect bcc supercells for Ti and Mo.

(2) Supercells with one vacancy (initial and final position, separated by one bond length) were relaxed to their ground state in the traditional way for Mo and Ta, while the structure for Ti was determined as described in Sec. II D. Then, the CI-NEB (Sec. II B) was used to determine the saddle point configuration for Mo and Ta, while Ti was again gained from the interpolation procedure.

(3) The lattice constants calculated in (1) were assigned to the ground state and transition state (saddle point) structures for Mo and Ti determined in (2).

(4) Γ-point phonon calculations using a finite difference method with displacements as described in Sec. II C were performed for all temperature-dependent structures, along with zero-temperature total energies.

(5) Self-diffusion coefficients at different temperatures were calculated based on the results from (4) using Eqs. (4)–(7).

(6) Analysis of the source of the nonlinearity of the diffusion coefficient was carried out by quantifying the nonlinearity of its different components in Eq. (4).

H. Computational details

First-principles calculations were employed to perform all structural relaxations and CI-NEB runs as well as energy and phonon-frequency calculations. To describe ion-electron interactions, we used projector augmented plane-wave potentials [45] as implemented in the Vienna *ab initio* simulation package (VASP), version 5.4.1 [45,46]. Exchange and correlation contributions to the total energy were described by the Perdew-Burke-Ernzerhof (PBE) functional [47]. After convergence tests, we chose a 54-atom supercell ($3 \times 3 \times 3$ conventional bcc unit cells) with $4 \times 4 \times 4$ Monkhorst-Pack k-point mesh for Brillouin zone integration. Cutoff energies of 300 eV for Mo and 700 eV for Ti were found to be necessary for convergence in the phonon calculations. For Ta, the cutoff energy was 300 eV as well. The settings were kept constant for all runs.

III. RESULTS AND DISCUSSION

A. Thermal expansion in Mo and β-Ti

The results from the quasiharmonic approximation for the Helmholtz free energy vs volume for temperatures between 0 and 1800 K in steps of 200 K for Mo and β-Ti are shown in Fig. 2(a). The energy minima are determined by a fit based on the assumption of a harmonic dependence of energy on the volume and are indicated by open markers in the plot at the minima of the parabolas. The minimum-energy lattice constants for both materials as a function of temperature are shown in Fig. 2(b).

The results for thermal expansion in Mo, based on traditional phonon calculations, are shown in Fig. 2(b). Fitting Eq. (10) to the DFT data results in parameter values of $a_0 = 3.1514$ Å, $\theta_D = 327$ K, $I_a = 5.91 \times 10^{-6}$ K^{-1}, and $\chi = 6.42 \times 10^{-6}$ K^{-1}. The lattice constant at 298 K is calculated with Eq. (10) to be 3.155 Å, while the experimental lattice constant at room temperature is 3.147 Å. The thermal expansion coefficient of Mo is calculated from the temperature derivative of Eq. (10) and is shown in Fig. 2(c) in comparison to experimental data from Ref. [48]. While the (weak) increase with temperature in the calculations is slightly lower than what is found in experiment, the general agreement is rather good with an average deviation in the linear regime between 600 and 1800 K of 5%.

The results for β-Ti, which are based on phonon calculations from the LDM, are shown in Fig. 2(a) and Fig. 2(b). Since, as described in Sec. II C, the LDM uses the harmonic envelope of the quartic energy-vs-displacement curve irrespective of whether or not the kinetic energy of the vibrating atoms is high enough to overcome the energy "hump" at zero displacement, which in the real system only happens above the transition temperature, it can also be used to calculate the energy vs volume dependence of metastable β-Ti below

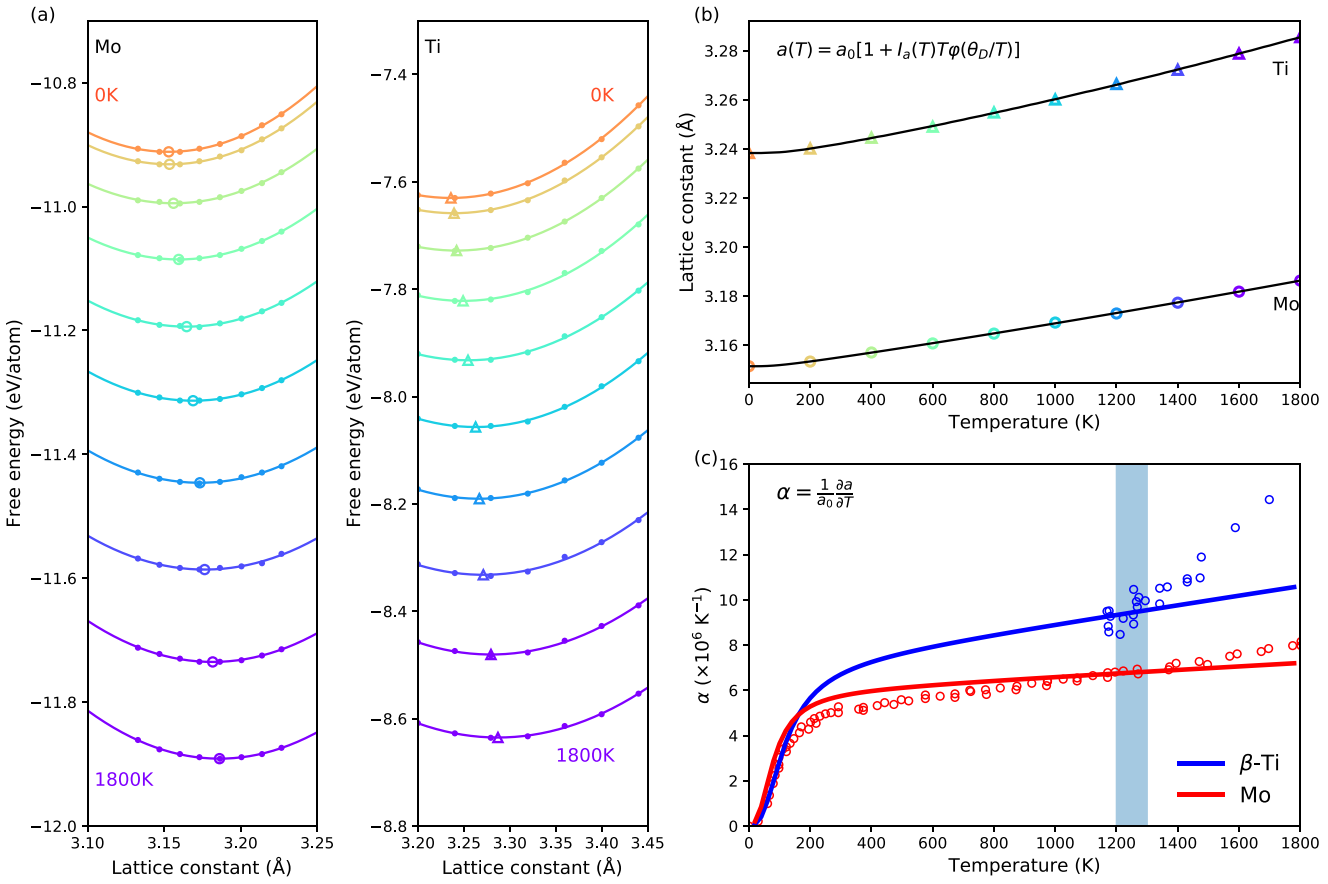

FIG. 2. (a) Free energy for bcc Mo and bcc Ti with respect to lattice constant at temperatures from 0 to 1800 K with 200 K step are depicted by solid circles. The values are fitted by quadratic curves (solid lines). Open markers denote the energy minima of the respective curves and simultaneously the equilibrium lattice constants. (b) Ground state lattice constants as a function of temperature for Mo (triangles) and β-Ti (circles), determined from the minima of the parabolic fits to DFT calculations of the Helmholtz free energy in panel (a) with the same color scheme. (c) Calculated thermal expansion for β-Ti (blue, upper line and data) and Mo (red, lower line and data). The lines are determined by fitting the DFT data from panel (b) with Eq. (10) and taking the temperature derivative. The circles denote experimental data from Ref. [48] for Mo and Ref. [49] for β-Ti.

the transition temperature and thus is shown here for the entire range. As seen in Fig. 2(a), the calculated values are well described by a quadratic fit for all temperatures, as was the case for Mo. Thus, we can use the entire range for fitting Eq. (10) to get more reliable coefficients and find parameters of $a_0 = 3.2383$ Å, $\theta_D = 474$ K, $I_a = 7.08 \times 10^{-6}$ K^{-1}, and $\chi = 1.47 \times 10^{-4}$ K^{-1}.

Experimental values compiled in Ref. [49] are for pure Ti only available above the transition temperature from α-Ti to β-Ti, which we have calculated previously to be at 1200 K with the LDM [30], within 4% of the experimental value of 1155 K. The calculated lattice constant of the β-Ti phase at 1200 K is 3.27 Å, compared to an experimental value at the same temperature of 3.33 Å. The calculated linear thermal expansion coefficient aligns well with the experimental values between 1200 and 1300 K with a considerable temperature dependence of $d\alpha/dT = 2 \times 10^{-10}$ K^{-2} [Fig. 2(c)]. For higher temperatures, it seems that anharmonic effects other than large displacements become important as already discussed in Ref. [30], causing a faster increase in thermal expansion in experiment than captured by LDM alone, which is one of the temperature limits for the applicability of the QHA [50], with the other being 2/3 of the melting temperature of 1941 K [51,52], which is also ∼1300 K. Therefore, we restrict our calculations here to this temperature range.

Overall, we have successfully determined the temperature dependence of the lattice constants, which agrees with experiments, and thus gives us reliable input for the following vacancy and diffusion-coefficient calculations.

B. Ground state of vacancy structure in β-Ti

Following the procedure described in Sec. II D, we have performed free-energy calculations of vacancy formation energies in constant-volume cells of β-Ti [lattice constant the zero-temperature value from Fig. 2(b), 3.237 Å] for three different temperatures (1155 K (experimental transition temperature), 1941 K (experimental melting point), and 1548 K (halfway in between) as a function of simultaneous nearest-neighbor displacement along the bond direction to the vacancy [Fig. 3(b)]. For each temperature, the minimum-energy displacement and energy minimum were determined from a parabolic fit. The results are shown in Fig. 3(a).

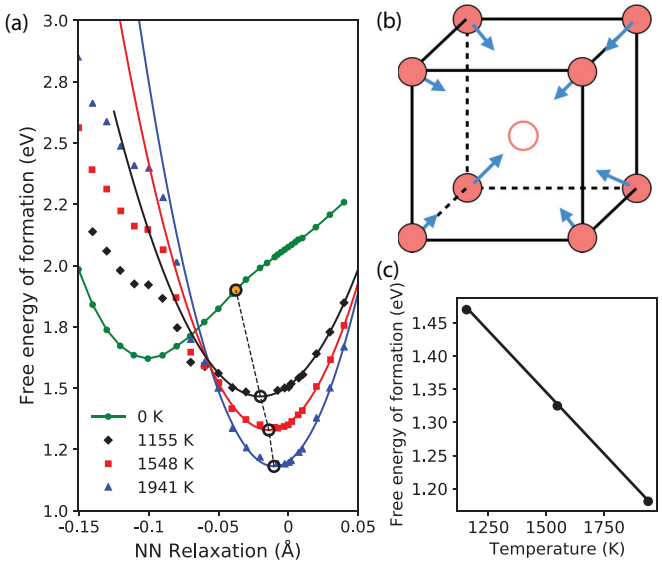

FIG. 3. (a) Free energy of formation for a vacancy in a 54-atom supercell of β-Ti as a function of simultaneous nearest-neighbor relaxation along the {111} bond directions [illustrated in (b)] with other atoms in fixed perfect lattice sites. Calculations were performed with DFT within the LDM quasiharmonic approximation. The symbols are calculation results for 1155 K (black diamonds, experimental transition temperature), 1941 K (blue triangles, experimental melting temperature), and 1548 K (red squares, halfway in between) with corresponding parabolic fits to find the minimum-energy displacements. The green circles are zero-temperature results, and the orange dot is the linear extrapolation vs temperature from the high-temperature minimum-energy displacements (hollow black circles along the dashed line) to the zero-temperature curve. (b) The nearest-neighbor displacement directions, with negative values moving toward the site of the vacancy (empty sphere). (c) Minimum-displacement free energy of formation [indicated by the hollow circles in (a)] for a vacancy in a 54-atom supercell of β-Ti as a function of temperature (circles), along with a linear fit with $F(T) = 1.90\ \text{eV} - 4.3k_BT$.

Figure 3(c) shows the free energy of formation as a function of temperature for the three calculation temperatures. In principle, the calculations performed here result in the Helmholtz free energy of formation at constant volume. In order to estimate the energy error with respect to the Gibbs free energy from the nonzero pressure that comes from neglecting the formation volume of the vacancy [30], we estimate the formation volume from the pressure in the VASP output for the NN-displaced cell and the bulk modulus and pressure derivative reported previously [30] through the pressure expression of the Murnaghan equation [53]. We find typical pressures of <10 kbar, indicating a volume relaxation in the supercell by less than 1%. Multiplying the formation volume from that with the pressures, we find that the pV term contributes less than 0.04 eV to the free energy, thus is small. Fitting $F(T) = E_f - TS$ to the three values, we find $E_f = 1.90$ eV and $S_f = 4.3k_B$. Combining these results with the lattice site density, we find an equilibrium vacancy concentration of $C^{\text{eq}}_{V,\text{Ti}} = 1.8 \times 10^{21}\ \text{cm}^{-3} \exp\{-1.90[\text{eV}]/(k_BT)\}$. For the unrelaxed cell, we had previously found with the same method $E_f = 2.05$ eV and $S_f = 8.15k_B$ [30]. Overall, the NN relaxation decreases the formation energy by 0.15 eV.

Next, we examine the NN relaxation as a function of temperature and extrapolate from it a zero-temperature displacement which can be used for a fully relaxed surrogate structure with all neighbor shells relaxed. Having three temperatures, extrapolation can either be done linearly [dashed line in Fig. 3(a)] or with a second-degree polynomial. We perform here both and take their average for our zero-temperature structure. For a linear extrapolation, we find a zero-temperature displacement of -0.035 Å, for a quadratic one -0.058 Å, with an average of -0.047 Å. All of these are considerably smaller than the minimum-energy zero-temperature relaxation of -0.101 Å, which is another expression of the mechanical instability of the structure and its strong stabilization by entropy. Following the procedure described in Sec. II D of interpolating fully relaxed cells of mechanically stable Mo and Ta vacancies with scaled lattice constants, which have NN relaxations of -0.008 Å and -0.082 Å in cells with otherwise clamped other neighbors, we then create a "relaxed" β-Ti cell which is more or less the straight average of the atomic positions in relaxed Mo and Ta cells, scaled to the β-Ti lattice constant. Both ground state structure and saddle point configuration were determined this way.

The formation energy from this process agrees with the formation energy from the interpolated structure discussed in Sec. II D within 0.01 eV, which is less than the uncertainties in our numbers from the different approximations and numerical calculations such as the 0.04 eV from enthalpy discussed in the present section. This suggests that relaxation beyond nearest neighbors adds only small changes to the calculated formation energies.

C. Self-diffusion in Mo

Our self-diffusion coefficients for Mo calculated within the quasiharmonic transition state theory are shown with previous experimental data [54–56] in Fig. 4(a). Our quasiharmonic transition state theory (qhTST) calculations with varying lattice constants that include thermal expansion are represented by the six individual points (1400–1900 K, with 100 K steps). We limit our highest calculated temperature to two-third of its melting point, one of the commonly accepted applicability range limits for QHA [51].

To further quantify the degree of nonlinearity in our data, we use Sec. II F to determine the deviation from linear $\ln D$ vs $1/T$ dependence, and then show that the normalized quadratic approximation suggested in Eqs. (11) and (12) is a satisfactory way to quantify the nonlinearity. In order to visualize the deviation from linearity, we adopt the concept of "enthalpy of mixing" and apply it to the $\ln D$ data. For that, we subtract the linear interpolation between highest and lowest values from the raw $\ln D$ data,

$$\Delta \ln D(\beta) = \ln D(\beta) - \frac{\beta - \beta_l}{\beta_h - \beta_l}\ln D_h - \frac{\beta_h - \beta}{\beta_h - \beta_l}\ln D_l, \quad (13)$$

which then automatically sets the high- and low-temperature end points to zero. Next, we use the interval normalization shown in Eq. (12) to $\Delta \ln D(\beta)$ in order to normalize the different temperature intervals to the same scale as described

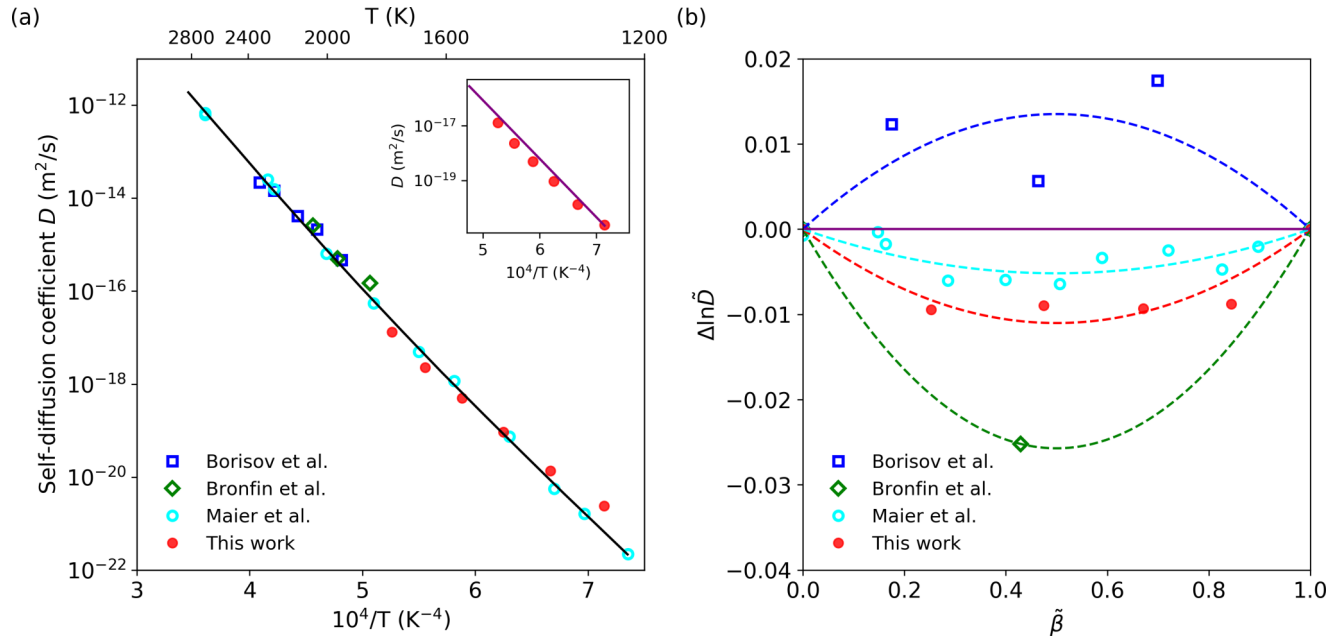

FIG. 4. Nonlinear Arrhenius self-diffusion in Mo. (a) Comparison between calculated self-diffusion coefficient D and experimental data from Refs. [54–56]. The solid line represents a parabolic fit of the experimental data by Maier *et al.* [56] to guide the eye. Inset: Comparison of D computed with (red markers as in main figure) and without (purple line) thermal expansion. (b) Nonlinearity plot of the normalized self-diffusion coefficient $\Delta \ln \tilde{D}$ [Eq. (14)] vs normalized temperature parameter $\tilde{\beta}$ [Eq. (15)] for the data from (a). The dashed curves are $\Delta \ln \tilde{D}_{\rm fit}(\tilde{\beta}) = \lambda\tilde{\beta}(1-\tilde{\beta})$ fits to determine λ. The purple flat line with zero curvature is for the harmonic approximation result from the inset of (a).

in Ref. [33],

$$\Delta \ln \tilde{D}(\beta) = \frac{\Delta \ln D(\beta)}{\sqrt{30}|\ln D_h - \ln D_l|}. \tag{14}$$

As before, $\beta = 1/(k_B T)$. We therefore display the deviation in the self-diffusion coefficients vs the normalized temperature given by

$$\tilde{\beta} = \frac{\beta - \beta_l}{\beta_h - \beta_l}. \tag{15}$$

The resulting plot is shown in Fig. 4(b), along with the Arrhenius plot of the same data sets in Fig. 4(a). Assuming lowest-order nonlinearity as expressed in Eq. (11), we fit the normalized $\ln D$ and $1/T$ data with the relation $\Delta \ln \tilde{D}_{\rm fit}(\tilde{\beta}) = \lambda\tilde{\beta}(1-\tilde{\beta})$, shown by the dashed lines in Fig. 4(b). The fitted nonlinearity parameter is $\lambda = -0.044$ for our work. Figure 4 further shows that eliminating the thermal expansion effect leads to the perfect Arrhenius dependence [purple line in the inset of Fig. 4(a)] and thus zero deviation from the linear term contribution [purple flat line in Fig. 4(b)]. This strongly suggests that thermal expansion is the crucial ingredient in our approach to correctly model the nonlinearity in the diffusion behavior of bcc Mo. While our absolute data are on the same order of magnitude with the experimental results in Fig. 4(a), they have a somewhat higher degree of nonlinearity than the rather expansive set of experimental values of Maier *et al.* [56], for which we calculate $\lambda = -0.021$. There is a larger uncertainty for the data sets of Bronfin *et al.* [55] and Borisov *et al.* [54] because of their small size and limited temperature range, for which we find $\lambda = -0.102$ and $\lambda = 0.054$, respectively, spanning a wide range.

In order to explore the origin of the bowing anomaly, we now investigate the temperature dependence of formation and migration enthalpies, as well as of formation entropy and attempt frequency. The results are shown in Figs. 5(a), 5(b)

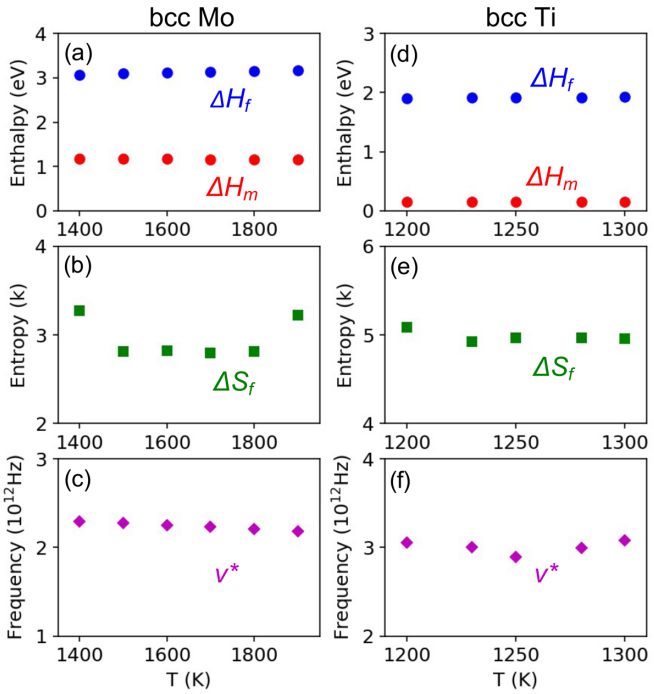

FIG. 5. Formation enthalpy ΔH_f, migration enthalpy ΔH_m, formation entropy ΔS_f, and diffusion attempt frequency ν^* for Mo [(a), (b), (c)] and β-Ti [(d), (e), (f)], calculated with DFT within quasiharmonic transition state theory.

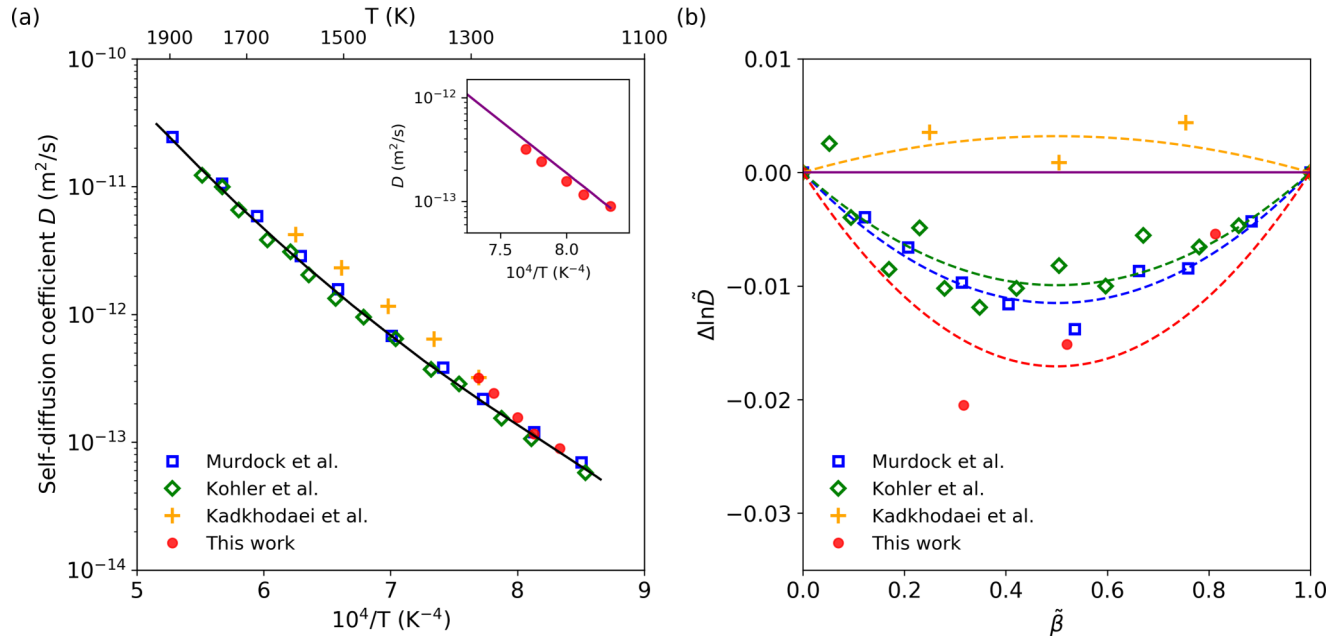

FIG. 6. Nonlinear Arrhenius self-diffusion in β-Ti. (a) Comparison between calculated self-diffusion coefficients D and experimental data from Refs. [14] and [57], as well as recent computational work from Ref. [17]. The solid line represents a parabolic fit of the experimental data to guide the eye. Inset: Comparison of D computed with (red markers as in main figure) and without (purple line) thermal expansion. (b) Nonlinearity plot of the normalized self-diffusion coefficient $\Delta \ln \tilde{D}$ [Eq. (14)] vs normalized temperature parameter $\tilde{\beta}$ [Eq. (15)] for the data from (a). The dashed curves are $\Delta \ln \tilde{D}_{\rm fit}(\tilde{\beta}) = \lambda\tilde{\beta}(1-\tilde{\beta})$ fits to determine λ. The purple flat line with zero curvature is for the harmonic approximation result from the inset of (a).

and 5(c). The calculated vacancy formation enthalpy ΔH_v increases monotonically with temperature from 3.08 eV to 3.17 eV between 1400 and 1900 K [Fig. 5(a)] and is slightly larger than values proposed from experiments of 3.0 eV [58]. The calculated vacancy migration enthalpy ΔH_m decreases slightly from 1.167 eV to 1.163 eV [Fig. 5(a)], slightly smaller than the reported migration enthalpy of 1.30 eV from experimental analysis [58]. The calculated attempt frequency ν^* also shows small temperature dependence and only decreases from 2.3×10^{12} Hz to 2.2×10^{12} Hz as temperature increases from 1400 to 1900 K [Fig. 5(c)]. On the other hand, the temperature dependence of the calculated vacancy formation entropy ΔS_f shows a much more pronounced temperature dependence and is found to be the major reason for non-Arrhenius-like diffusion in Mo. It decreases from $3.27k_B$ at 1400 K to $2.79k_B$ at 1700 K, before recovering back to $3.22k_B$ at 1900 K, as shown in Fig. 5(b). The curved shape of $\Delta S_f(T)$ then directly progresses into the curvature of the calculated self-diffusion coefficients in Fig. 4. In order to quantify the effect of the different contributions, we perform two fits of Eq. (11), first one for calculated diffusion coefficients where the prefactor is fixed to the average value of all calculated prefactors (which results in a value of $D_0^{\rm avg} = 3.25 \times 10^{-6}$ m^2/s), and second an analogous set of diffusion coefficients where the activation energy is fixed to the average calculated value of $E_0^{\rm avg} = 4.268$ eV. For the first fit, we find almost zero nonlinearity, while for fixed E_a, we find $\lambda = -0.041$, which is 93% of the overall nonlinearity. Thus, the nonlinearity in vacancy diffusion in Mo is clearly dominated by the nonlinearity of the diffusion prefactor as a consequence of anharmonicity from thermal expansion. To investigate the effect further, a similar analysis was made with fixed averaged attempt frequency, resulting in a change of nonlinearity by less than 1%, making the nonlinearity in the formation entropy by far the most important factor.

This conclusion is different from the DFT-MD calculation by Mattsson *et al.* [18], in which the anomaly was mostly attributed to anharmonicity in the vacancy formation enthalpy ΔH_v. In their simulations, thermal expansion was not considered and all MD simulations were performed at the zero-temperature volume of vacancy and bulk, which neglected important volume-dependent anharmonic effects from thermal expansion. The fundamental proportionality between the Grüneisen parameter, the prime indicator for anharmonicity, and thermal expansion [41] as well as our results here are strong indicators that thermal expansion cannot be neglected when trying to understand anharmonic effects. Our findings are further supported by the resistivity measurements by Schwirtlich and Schultz [59], who find the temperature dependence of the formation enthalpy is small and constant to within 0.1 eV between 2000 K and 2600 K, whereas Mattson *et al.* predict a much larger increase of 0.5 eV for that interval.

D. Self-diffusion in β-Ti

Our calculation results of self-diffusion coefficients in β-Ti are plotted in Fig. 6(a) in comparison to both experimental and computational data [15,17,57]. Calculations based on TST and the large-displacement algorithm are applied at five temperatures: 1200, 1230, 1250, 1280, and 1300 K. As already described in Sec. III A, we choose the lower limit of 1200 K as the α-to-β transition temperature from LDM-DFT calculations [30]. As to the higher limit, both the divergence between experimental and theoretical thermal expansion coef-

ficient as well as the 2/3 melting-temperature cutoff limit the QHA applicability range to <1300 K [50–52]. Although these choices make the temperature range for the DFT calculations rather small, the anomaly of the self-diffusion coefficient can still be seen in Fig. 6(b), and the data are sufficient to extract the nonlinearity parameter, which is independent of the temperature interval as we have discussed earlier.

To compare the nonlinearity of the self-diffusion in bcc Ti, we plotted the normalized $\Delta \ln \tilde{D}$ vs $\tilde{\beta}$ in Fig. 6(b), taking a procedure similar to that in Sec. III C. From the LDM-DFT calculations, we find for β-Ti a nonlinearity coefficient of $\lambda = -0.068$, about 1.6 times than what we had found for Mo. A similarly stronger nonlinearity is also found in experiments, where we fit a nonlinearity parameter of $\lambda = -0.045$ for Murdock *et al.* [57], and $\lambda = -0.040$ for Kohler *et al.* [14], which is about 2 times the Mo value.

In contrast to these positive normalized curvature parameters, the computational results from Kadkhodaei *et al.* [17] show a small but positive nonlinearity parameter of $\lambda = 0.012$. This is a *qualitative* discrepancy since the comprehensive theoretical approach Kadkhodaei *et al.* should have accounted for all contributions from lattice anharmonicity at different temperatures except for the effect from thermal expansion since the same volume was used for all temperatures. To further demonstrate the significance of thermal expansion, we performed the same calculations with fixed volume at the low-temperature limit. As shown in the inset of Fig. 6(a) and the purple flat line in Fig. 6(b), the $\ln D$ vs. $1/T$ dependence is perfectly linear. This striking contrast is a strong indication that thermal expansion is the most likely cause for the negative nonlinearity parameter λ in the anomalous diffusion behavior in β-Ti. In order to explore whether the origins of the bowing anomalies in β-Ti and Mo differ, we again investigate the temperature dependence of formation and migration enthalpies, as well as of formation entropy and attempt frequency. The results are shown in Figs. 5(d), 5(e) and 5(f). The vacancy formation enthalpy ΔH_f increases from 1.91 eV to 1.92 eV at the temperature from 1200 K to 1300 K [Fig. 5(d)], compared with an experimental estimation of >1.50 eV [60]. This value from interpolated Mo and Ta zero-temperature cells (Secs. II D and III B) agrees well with the results from the nearest-neighbor-only free-energy minimization, where the nearly perfect linearity with temperature indicated a very weak temperature dependence of the formation enthalpy [Fig. 5(d)]. Similarly, the vacancy migration enthalpy ΔH_m increases only slightly from 0.146 eV to 0.147 eV as temperature increases [Fig. 5(d)]. Indeed, when we fit the calculated diffusion coefficients once again with an averaged prefactor (which has a value of $D_0^{\text{avg}} = 3.403 \times 10^{-5}$ m^2/s for β-Ti), we find a slightly positive nonlinearity. Thus, it is once again the prefactor that we identify as the major source (90%) of the nonlinearity with $\lambda = -0.0616$. Unlike Mo, however, both vacancy formation entropy and attempt frequency contribute to a more comparable degree to the nonlinear Arrhenius curve in β-Ti. Specifically, the vacancy formation entropy ΔS_f decreases from $5.08k_B$ at 1200 K to a minimum of $4.92k_B$ at 1230 K before increasing back to $4.95k_B$ at 1300 K [Fig. 5(e)], and the attempt frequency ν^* decreases from 3.1×10^{12} Hz at 1200 K to 2.9×10^{12} Hz at 1250 K, then increases back to 3.1×10^{12} Hz at 1300 K [Fig. 5(f)]. With that, the formation entropy carries 64% of the nonlinearity, leaving the remaining 36% to the attempt frequency. Without the anharmonic attempt frequency, the calculated nonlinearity in β-Ti would only be 25% larger than that in Mo, and thus the effect of the formation entropy is rather comparable in both materials.

IV. CONCLUSIONS AND OUTLOOK

In summary, we have demonstrated that the nonlinear Arrhenius self-diffusion behavior in bcc metals for the examples of Mo and β-Ti can be largely attributed to the thermal expansion effect, using the framework of quasiharmonic transition state theory. In order to be able to calculate phonon frequencies needed for attempt frequency and formation entropy in the mechanically unstable β-Ti, we use the previously proposed large-displacement method and introduce a two-step approach for structural relaxation in mechanically unstable crystals, which is first free-energy relaxation of the nearest-neighbor shell and second further refinement by interpolation of relaxed stable structures weighted by the nearest-neighbor displacements. We also use a modified Debye formula to fit thermal expansion over the entire temperature range allowing prediction of lattice constants for any elevated temperature from a few explicit calibration QHA calculations. We find that phonon frequencies, at the heart of the two quantities that define the diffusion prefactor—vibrational entropy and attempt frequency—are greatly affected by thermal expansion, and further lead to a *nonlinear* $\ln D$ vs $1/T$ dependence. In order to quantify the degree of such nonlinearity in both bcc Mo and β-Ti, we formulated a nonlinearity parameter λ with respect to normalized diffusion coefficients at various temperature ranges, and compare our results with previous experimental data and computational work. β-Ti shows much stronger nonlinearity than bcc Mo, and we further find a considerable difference in the distribution of the nonlinearity on formation entropy: While nearly all of the nonlinearity in Mo comes from the formation entropy, the nonlinearity in β-Ti is divided 2/3 : 1/3 between formation entropy and attempt frequency, respectively, in contrast to previous suggestions. The nonlinearity analysis of our calculated diffusion coefficients indicates that thermal expansion is largely responsible for the deviation from linear Arrhenius-type self-diffusion in bcc metals. Finally, our proposed methodology is general enough that it also can be applied to other crystals with similar mechanical instability.

ACKNOWLEDGMENTS

This work is primarily supported by the U.S. National Science Foundation (NSF) under Grant No. CMMI-1333999 (Z.Q.C. and J.-C.Z.), and it is part of an NSF Designing Materials to Revolutionize and Engineer our Future (DMREF) project. J.-C.Z. also acknowledges NSF under Grant No. 1904245 that continues his study on diffusion in metals. Computer calculations were performed at the Ohio Supercomputer Center under Grants No. PAS0551 and No. PAS0072. Y.W. and W.W. acknowledges funding from AFOSR under Program Director Dr. Ali Sayir through Project No. FA9550-19-1-0378.

[1] G. Neumann and C. Tuijn, *Self-Diffusion and Impurity Diffusion in Pure Metals: Handbook of Experimental Data* (Elsevier, 2011).

[2] A. Da Fano and G. Jacucci, Vacancy Double Jumps and Atomic Diffusion in Aluminum and Sodium, Phys. Rev. Lett. **39**, 950 (1977).

[3] M. Ait-Salem, A. Springer, T Heidemann, and B. Alefeld, Investigation of the self-diffusion in solid sodium using quasielastic neutron scattering, Philos. Mag. A **39**, 797 (1979).

[4] G. Göltz, A. Heidemann, H. Mehrer, A. Seeger, and D. Wolf, Study of atomic jump processes in sodium crystals by quasi-elastic neutron scattering, Philos. Mag. A **41**, 723 (1980).

[5] W. Schilling, Self-interstitial atoms in metals, J. Nucl. Mater. **69**, 465 (1978).

[6] J. M. Sanchez and D. de Fontaine, Model for Anomalous Self-Diffusion in Group-IVB Transition Metals, Phys. Rev. Lett. **35**, 227 (1975).

[7] J. Sanchez and D. D. Fontaine, Anomalous diffusion in omega forming systems, Acta Metall. **26**, 1083 (1978).

[8] C. Herzig and U. Köhler, Anomalous self-diffusion in BCC IVB metals and alloys, Mater. Sci. Forum **15**, 301 (1987).

[9] W. Petry, T. Flottmann, A. Heiming, J. Trampenau, M. Alba, and G. Vogl, Atomistic Study of Anomalous Self-Diffusion in bcc β-Titanium, Phys. Rev. Lett. **61**, 722 (1988).

[10] G. Vogl, W. Petry, T. Flottmann, and A. Heiming, Direct determination of the self-diffusion mechanism in bcc β-titanium, Phys. Rev. B **39**, 5025 (1989).

[11] G. Neumann, C. Tuijn, G. de Vries, and H. Bakker, Diffusion mechanisms in B.C.C. metals: Calculation of the correlation factor for mixed nearest and next-nearest neighbour vacancy jumps, Phys. Status Solidi B **149**, 483 (1988).

[12] M. Rieth and W. Schommers, *Handbook of Theoretical and Computational Nanotechnology. Nanodevice Modeling and Nanoeletronics* (American Scientific Publishers, 2007), Vol. 10, pp. 137–209.

[13] N. Stoddard, P. Pichler, G. Duscher, and W. Windl, *Ab Initio* Identification of the Nitrogen Diffusion Mechanism in Silicon, Phys. Rev. Lett. **95**, 025901 (2005).

[14] U. Köhler and C. Herzig, On the anomalous self-diffusion in bcc titanium, Phys. Status Solidi B **144**, 243 (1987).

[15] U. Köhler and C. Herzig, On the correlation between self-diffusion and the low-frequency LA $\frac{2}{3}\langle 111\rangle$ phonon mode in bcc metals, Philos. Mag. A **58**, 769 (1988).

[16] G. Smirnov, Non-Arrhenius diffusion in bcc titanium: Vacancy-interstitialcy model, Phys. Rev. B **102**, 184110 (2020).

[17] S. Kadkhodaei and A. Davariashtiyani, Phonon-assisted diffusion in bcc phase of titanium and zirconium from first principles, Phys. Rev. Materials **4**, 043802 (2020).

[18] T. R. Mattsson, N. Sandberg, R. Armiento, and A. E. Mattsson, Quantifying the anomalous self-diffusion in molybdenum with first-principles simulations, Phys. Rev. B **80**, 224104 (2009).

[19] D. G. Sangiovanni, J. Klarbring, D. Smirnova, N. V. Skripnyak, D. Gambino, M. Mrovec, S. I. Simak, and I. A. Abrikosov, Superioniclike Diffusion in an Elemental Crystal: Bcc Titanium, Phys. Rev. Lett. **123**, 105501 (2019).

[20] E. Fransson and P. Erhart, Defects from phonons: Atomic transport by concerted motion in simple crystalline metals, Acta Mater. **196**, 770 (2020).

[21] W.-S. Ko, B. Grabowski, and J. Neugebauer, Development and application of a Ni-Ti interatomic potential with high predictive accuracy of the martensitic phase transition, Phys. Rev. B **92**, 134107 (2015).

[22] R. G. Hennig, T. J. Lenosky, D. R. Trinkle, S. P. Rudin, and J. W. Wilkins, Classical potential describes martensitic phase transformations between the α, β, and ω titanium phases, Phys. Rev. B **78**, 054121 (2008).

[23] D. Dickel, C. D. Barrett, R. L. Carino, M. I. Baskes, and M. F. Horstemeyer, Mechanical instabilities in the modeling of phase transitions of titanium, Modell. Simul. Mater. Sci. Eng. **26**, 065002 (2018).

[24] W. Windl, M. M. Bunea, R. Stumpf, S. T. Dunham, and M. P. Masquelier, First-Principles Study of Boron Diffusion in Silicon, Phys. Rev. Lett. **83**, 4345 (1999).

[25] H. Wu, T. Mayeshiba, and D. Morgan, High-throughput ab-initio dilute solute diffusion database, Sci. Data **3**, 160054 (2016).

[26] T. Angsten, T. Mayeshiba, H. Wu, and D. Morgan, Elemental vacancy diffusion database from high-throughput first-principles calculations for fcc and hcp structures, New J. Phys. **16**, 015018 (2014).

[27] M. Mantina, Y. Wang, R. Arroyave, L. Q. Chen, Z. K. Liu, and C. Wolverton, First-Principles Calculation of Self-Diffusion Coefficients, Phys. Rev. Lett. **100**, 215901 (2008).

[28] M. Mantina, Y. Wang, L. Chen, Z. Liu, and C. Wolverton, First principles impurity diffusion coefficients, Acta Mater. **57**, 4102 (2009).

[29] M.-X. Wagner and W. Windl, Lattice stability, elastic constants and macroscopic moduli of NiTi martensites from first principles, Acta Mater. **56**, 6232 (2008).

[30] N. Antolin, O. D. Restrepo, and W. Windl, Fast free-energy calculations for unstable high-temperature phases, Phys. Rev. B **86**, 054119 (2012).

[31] O. Hellman, I. A. Abrikosov, and S. I. Simak, Lattice dynamics of anharmonic solids from first principles, Phys. Rev. B **84**, 180301(R) (2011).

[32] P. Souvatzis, O. Eriksson, M. Katsnelson, and S. Rudin, The self-consistent ab initio lattice dynamical method, Comput. Mater. Sci. **44**, 888 (2009).

[33] K. Emancipator and M. H. Kroll, A quantitative measure of nonlinearity, Clin. Chem. **39**, 766 (1993).

[34] G. L. Montet, Integral methods in the calculation of correlation factors in diffusion, Phys. Rev. B **7**, 650 (1973).

[35] K. Compaan and Y. Haven, Correlation factors for diffusion in solids, Trans. Faraday Soc. **52**, 786 (1956).

[36] G. H. Vineyard, Frequency factors and isotope effects in solid state rate processes, J. Phys. Chem. Solids **3**, 121 (1957).

[37] S. Baroni, S. de Gironcoli, A. Dal Corso, and P. Giannozzi, Phonons and related crystal properties from density-functional perturbation theory, Rev. Mod. Phys. **73**, 515 (2001).

[38] W. Luo and W. Windl, First principles study of the structure and stability of carbynes, Carbon **47**, 367 (2009).

[39] J. C. Slater, *Introduction to Chemical Physics* (McGraw-Hill, 1939).

[40] G. Henkelman, B. P. Uberuaga, and H. Jónsson, A climbing image nudged elastic band method for finding saddle points and minimum energy paths, J. Chem. Phys. **113**, 9901 (2000).

[41] F. Sayetat, P. Fertey, and M. Kessler, An easy method for the determination of Debye temperature from thermal expansion analyses, J. Appl. Crystallogr. **31**, 121 (1998).

[42] H. C. Thacher, Jr., Rational approximations for the Debye functions, J. Chem. Phys. **32**, 638 (1960).
[43] J. Dickinson and P. Armstrong, Temperature dependence of the elastic constants of molybdenum, J. Appl. Phys. **38**, 602 (1967).
[44] W. Windl, O. F. Sankey, and J. Menéndez, Theory of strain and electronic structure of $Si_{1-y}C_y$ and $Si_{1-x-y}Ge_xC_y$ alloys, Phys. Rev. B **57**, 2431 (1998).
[45] G. Kresse and D. Joubert, From ultrasoft pseudopotentials to the projector augmented-wave method, Phys. Rev. B **59**, 1758 (1999).
[46] G. Kresse and J. Hafner, *Ab initio* molecular dynamics for liquid metals, Phys. Rev. B **47**, 558 (1993).
[47] J. P. Perdew, K. Burke, and M. Ernzerhof, Generalized Gradient Approximation Made Simple, Phys. Rev. Lett. **77**, 3865 (1996).
[48] K. Wang and R. R. Reeber, The role of defects on thermophysical properties: Thermal expansion of V, Nb, Ta, Mo and W, Mater. Sci. Eng., R **23**, 101 (1998).
[49] Y. S. Touloukian, R. Kirby, R. Taylor, and P. Desai, *Thermophysical Properties of Matter, the TPRC Data Series, Thermal Expansion, Metallic Elements and Alloys* (Thermophysical and Electronic Properties Information Analysis Center, 1975), Vol. 12.
[50] B. B. Karki, R. M. Wentzcovitch, S. de Gironcoli, and S. Baroni, First principles thermoelasticity of $MgSiO_3$-perovskite: Consequences for the inferred properties of the lower mantle, Geophys. Res. Lett. **28**, 2699 (2001).
[51] M. Kotelyanskii and D. N. Theodorou, *Simulation Methods for Polymers* (CRC Press, 2004).
[52] J. M. Skelton, S. C. Parker, A. Togo, I. Tanaka, and A. Walsh, Thermal physics of the lead chalcogenides PbS, PbSe, and PbTe from first principles, Phys. Rev. B **89**, 205203 (2014).
[53] F. D. Murnaghan, The compressibility of media under extreme pressures, Proc. Natl. Acad. Sci. USA **30**, 244 (1944).
[54] Y. Borisov, P. Gruzin, L. Pavliniv, and G. Fedorov, Self-diffusion of molybdenum, Metall. Pure Met. Sci. **1**, 213 (1959).
[55] M. Bronfin, S. Bokshtein, and A. Zhukhovistsky, Self-diffusion in molybdenum, Zavod. Lab. **26**, 828 (1960).
[56] K. Maier, H. Mehrer, and G. Rein, Self-diffusion in molybdenum, Z. Metallkd. **70**, 271 (1979).
[57] J. Murdock, T. Lundy, and E. Stansbury, Diffusion of Ti_{44} and V_{48} in titanium, Acta Metall. **12**, 1033 (1964).
[58] H. Ullmaier (ed.), *Atomic Defects in Metals* (Springer-Verlag, 1991).
[59] I. Schwirtlich and H. Schultz, Quenching and recovery experiments on molybdenum, Philos. Mag. A **42**, 601 (1980).
[60] F. R. de Boer, W. Mattens, R. Boom, A. Miedema, and A. Niessen, *Cohesion in Metals: Transition Metal Alloys* (North-Holland, 1988).